Continuous and Responsive D2D Victim Localization for Post-Disaster Emergencies

Vishaka Basnayake[1,2], Hakim Mabed[1], Philippe Canalda[1], Dushantha Nalin K. Jayakody[3]
[1]*DISC/FEMTO-ST, Univ. Bourgogne Franche-Comte,* Cours Louis Leprince-Ringuet, 25200, Montbeliard, France
[2]*Centre for Telecommunication Research, School of Engineering, Sri Lanka Technological Campus,* 10500 Padukka, Sri Lanka
[3]*COPELABS Lusófona University* Lisbon 1700-097, Portugal
{vishaka.basnayake_mudiyanselage, hakim.mabed, philippe.canalda}@univ-fcomte.fr, nalin.jayakody@ieee.org

***Abstract*—One of the most challenging tasks in a disaster scenario is the detection and localization of victims with high accuracy and minimum delay, especially in out-of-coverage areas. In the event of a disaster that disrupts the cellular network infrastructure, emergency calls can be relayed to the core network via multi-hop D2D communications. In this paper, a localization system is proposed that uses radio measurements obtained through such D2D multi-hop assisted emergency calls to localize in-coverage and out-of-coverage devices. To address the uncertainty and gradual reception of data in real-time in this scenario, a dynamic constraint satisfaction-based Multi Victim Localization Algorithm *(MVLA)* is proposed. This algorithm locates multi-hop devices in a progressive propagation manner to provide fast and accurate updates on victim locations. Additionally, three modes of *MVLA*, namely $MVLA_{recent}$, $MVLA_{seq}$, and $MVLA_{all}$ are proposed. Simulation results demonstrate that $MVLA_{all}$ has a lower localization error compared to $MVLA_{recent}$ and $MVLA_{seq}$. Moreover, $MVLA_{all}$, is compared with an existing particle filtering-based localization algorithm called RSSI Monte-Carlo Boxed Localization (*RSSI-MCL*) under an increasing number of emergency user devices and functional gNodeBs. Results show that $MVLA_{all}$ significantly outperforms the *RSSI-MCL* method in terms of localization accuracy and computational delay.**

Index Terms*—Computational delay, Dynamic constraint satisfaction, D2D, Localization accuracy, Multi-victim localization algorithm, Out-of-coverage, *RSSI-MCL

I. Introduction

The advancements in technology, such as Global Navigation Satellite Systems (GNSS) [1]–[4], Multi-Input and Multiple-Output (MIMO) antennas [5], [6], and Device-to-Device (D2D) communications [7], have greatly improved the capabilities of smartphones in terms of communication, navigation, and positioning. These technologies are particularly useful for localization tasks during disaster scenarios, where it is important to locate victim devices with high accuracy and minimal delay in order to rescue them promptly [8], [9].

One such technology is D2D communication, which is made possible by the new direct link between User Equipment (UE) known as Sidelink defined at the access stratum layers. The Sidelink feature enables UEs to exchange information when they are in close proximity, even when the UEs are out of coverage, as per [10]. Also, out-of-coverage D2D, which operates independently of the core network, can be deployed via autonomous D2D interfaces such as Bluetooth, Wi-Fi Direct, or LTE D2D. Research studies have proposed using D2D-assisted multi-hop protocols to relay emergency calls from out-of-coverage areas to a core network, allowing for the collection of data for localization [11]–[16]. In this scenario, emergency calls are relayed by neighboring devices toward a functional eNodeB/gNodeB using D2D-assisted multi-hop relaying, as shown in Figure 1.

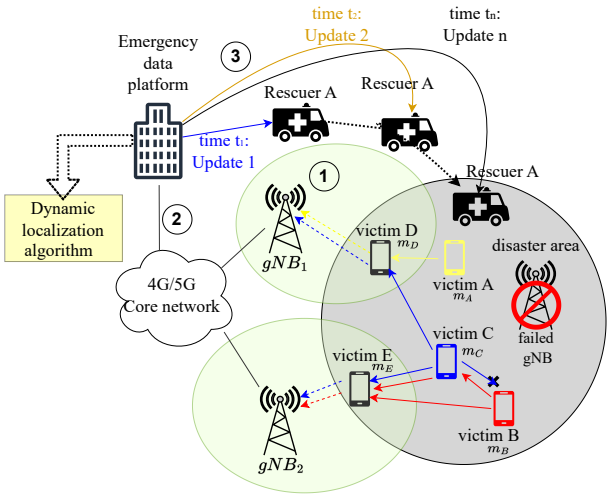

Figure 1: Target scenario: 1) Emergency UEs in the disaster area forward their calls in the direction of the functioning gNBs via relay UEs in the neighborhood. Distinct emergency calls are denoted by the arrow color. 2) Such calls arrive at an emergency platform to localize victims. 3) The resultant localization is updated dynamically in fixed time intervals for the rescuers who are searching for victims.

Next, localization can be accomplished via either homogeneous or hybrid methods [17], using measurement data obtained through multi-hop protocols. Homogeneous localization relies on one measurement source. Table. I shows the accuracy results obtained from practical experiments in related literature, which used homogeneous localization approaches such as Global Positioning System (GPS), Angle of Arrival

This research was funded by the Fundação para a Ciência e a Tecnologia, Portugal under the national funds through Grant No.: 2022.03897.PTDC and by the CEU-Cooperativa de Ensino Universitário, Portugal.

(AoA), Received Signal Strength Indicator (RSSI), and Time of Arrival (ToA).

Table I: Confidence intervals of GPS, RSSI, ToA and AoA localization approaches

Approach	Environment	Measurement error (min, max)	Citation
GPS	Outdoor (NLOS)	(5 - 99.7) m	[18]
GPS	Indoor Building (1-2 floors) (NLOS)	(1 - 2) m	[19]
GPS	Indoor Building ($>$ 2 floors) (NLOS)	(2 - 21.7) m	[19]
RSSI	NLOS	(1.5 - 5) m	[20], [21]
ToA	NLOS	(1 - 5.23) m	[22]
AoA	NLOS	$(\pi/18 - \pi/3)$ rad	[22], [23]

GPS-assisted localization uses signals from a network of satellites to determine the location of a device. The device uses trilateration to estimate its location based on the time delay between the transmission and reception of the satellite signals [24]. GPS offers high localization accuracy [25], but requires a minimum of four satellites in view, and consumes a lot of power, and has line of sight requirements [7]. Next, AoA-assisted localization determines the location of a device using the angles at which signals from multiple reference points arrive at the device [26]. The device must be equipped with MIMO antennas to measure the AoA [27]. Martin Schüssel shows that the AoA technique estimates the transmitter direction with an error of about 60^0 using a Nexus 5X smartphone equipped with a 2×2 MIMO antenna [23]. Table II lists commercially available smartphones with MIMO technology and their specifications.

Table II: Specifications of commercially available smartphones with MIMO

Smartphone	MIMO Model	Capacity	Price (eur)	Network
iPhone SE	2×2	64 - 256GB	399 - 600	LTE
iPhone XR	2×2	64 - 512GB	499 - 878	LTE
iPhone XS and XS max	4×4	64 - 512 GB	199 - 400	LTE
iPhone 12	4×4	64 - 256 GB	678 - 799	LTE/5G
Samsung's Galaxy S9 and S9+	4×4	64 - 256 GB	350 - 575	LTE
Samsung's Galaxy 21	4×4	64 - 256 GB	859 - 1149	LTE/5G
Google's Pixel 3 and Pixel 3 XL	4×4	64 - 128 GB	489 - 815	LTE
Google's Pixel 5	4×4	128 GB	629 - 700	LTE/5G

RSSI-assisted localization is a technique for finding the location of a device through the measurement of wireless signal strengths received from multiple reference points or transmitters [28], [29]. This method is less complex and cost-effective compared to other techniques as it doesn't need synchronization between the transmitter and receiver [30], [31]. RSSI values are calculated using an empirical propagation model and are used to estimate the distance between the transmitter and receiver [30], [32]. The location of the receiver is determined using this information, as well as factors such as the transmission signal power and path loss exponent. Next, ToA-assisted localization determines the location of a device based on the time it takes for a signal to travel from the transmitter to the receiver [30]. However, the accuracy of this technique can be affected by factors such as the accuracy of the transmitter/receiver clocks, the presence of obstacles or reflections, and multipath fading, making it less accurate than other techniques such as AoA or RSSI-assisted localization specially in out-of-coverage scenarios. ToA-based range computation requires synchronization between the transmitter and receiver and is therefore mostly used when the device is under gNodeB (gNB) coverage.

On the other hand, hybrid localization combines measurement types such as GPS, RSSI, ToA, and AoA. Hybrid localization approaches are used to improve the overall performance or to support an algorithm that cannot be applied standalone given the lack of signal measurements [33], [34]. With the increasing demand for high-accuracy positioning, hybrid signal-based localization is gaining more attention [35]. Experimental analysis in [7], [36] shows that hybrid localization approaches yield a higher accuracy compared to homogeneous localization. Moreover, in traditional localization methods, homogeneous or hybrid techniques are employed when there is a functional radio network infrastructure in place. These techniques involve combining the signals from devices received by the gNB to determine the positions of the target devices. On the other hand, in the event of a major disaster that disrupts the network infrastructure, the position of a target device is determined by utilizing ad-hoc D2D signals received from neighboring devices. Moreover, Figure 2 shows the difference between these classical and ad-hoc localization approaches.

Additionally, several localization algorithms have been proposed in literature including Particle Filtering (PF) [40], Least Squares Error (LSE) [37], Kalman Filtering, and Constraint Satisfaction Programming (CSP). Many research studies have used PF-based algorithms known as the Monte Carlo Localization (MCL) and Montecarlo Boxed Localization (MCB) [41], [43], [48]–[50]. However, the PF-based algorithm has a significant drawback which is its computational complexity that causes high memory usage and computational latency [40]. Moreover, the Extended Kalman Filter (EKF) is another localization algorithm that is based on the Kalman filter principles and assumes Gaussian uncertainty in the measurements [50], [51]. It is noted that, due to the incomplete knowledge regarding the measurement process, the assumption that the errors follow a known probability distribution such as Gaussian is less robust in the localizing process where the measurement errors can be considerably random [17]. In addition, such assumptions lead to more biased computations in the presence of repeated or sequential location estimations [17].

Table III: Comparison of major localization algorithms

Related Work	Progressive propagation of multi-hop device positioning	Control traffic	Number of reference nodes	Data availability	Deployed Localization Algorithm	Required Measurements or data
[37]	No	Yes	Medium	Fixed	Weighted Least Squares (WLS) assisted localization	RSSI+AoA
[38]	No	Yes	Medium	Fixed	EKF-based localization	RSSI+AoA
[39]	No	Yes	Medium	Fixed	MCL-assisted localization	RSSI
[40]	No	Yes	Medium	Fixed	PF-assisted localization	GPS+RSSI+AoA
[41]	No	Yes	Medium	Fixed	PF-assisted localization	GPS+RSSI
[42]	No	Yes	Medium	Fixed	MCB-assisted localization	GPS+RSSI
[43]	No	Yes	Medium	Fixed	MCB-assisted localization	GPS+RSSI
[44]	No	Yes	Medium	Fixed	CSP-assisted localization	GPS+AoA
[45]	No	Yes	Medium	Fixed	CSP-assisted localization	GPS+AoA
[46]	No	Yes	Low	Fixed	CSP-assisted localization	GPS+RSSI
[47]	No	Yes	Low	Fixed	CSP-assisted localization	GPS+AoA
Our approach	Yes	No	Very low (< 3)	Progressive	CSP-assisted localization	GPS+RSSI+ToA+AoA

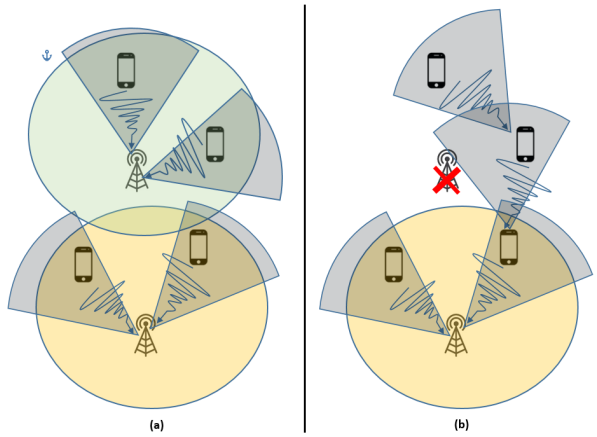

Figure 2: Comparison between (a) classical localization approach under operational network and (b) our localization approach under dysfunctional network. In the classical approach, the localization system uses the signals received by the base stations from the devices. In our case, the localization system uses mainly signals received by the devices from other devices. The sectors in the figure refer to the signal AoA estimation and the wavy arrows to the signal quality measured by the RSSI.

In comparing the MCL and EKF algorithms, it is observed that MCL has shown better localization accuracy when compared to the EKF method in the literature [50]. Further, it should be noted that a variation of MCL known as RSSI-based Monte-Carlo Boxed Localization (*RSSI-MCL*) has shown better positioning accuracy than MCL in [43]. Both MCL and MCB use the technique of Monte Carlo which is based on random sampling, to determine the position of a target device. It is to be noted that the main difference in MCB localization from MCL is due to using a bounded area as the search space for the target node's position.

Thirdly, the CSP-based algorithm has been used for robots and radio device localization tasks in private ad hoc context [44]–[47], [52]–[56]. Furthermore, techniques such as priority ordering, filtering, and iterative min-conflict methods have been used to enhance the performance of CSP algorithms [57]–[59]. Moreover, in comparison to EKF, the only assumption in the CSP algorithm is to verify that the errors are bounded within minimum and maximum limits. Additionally, the minimum and maximum error limits can be determined by analyzing the tolerance levels of measurements obtained via experimental data. It is important to note that assuming errors are bounded is a crucial assumption, but if this assumption is found to be invalid, there are techniques to eliminate the outliers [17]. Further, the localization based on Gaussian uncertainty has been shown to be inconsistent in terms of localization error compared to the CSP method [44]. Consistency in estimations can be significantly important in localization in real-world circumstances.

Moreover, comparing MCL and CSP algorithms, CSP has shown improved localization accuracy [52], [60]. CSP-based localization can apply constraints on the solution space to ensure that the estimated position is physically plausible and consistent with the available measurements. This allows CSP-based localization to produce more accurate and reliable results than MCL, which is based on random sampling. Nevertheless, the existing CSP algorithms have mainly focused on the use of anchor nodes whose actual locations are known with high confidence. Further, it is noted that the existing localization systems often rely on control signals that provide information for the localization of target devices. Additionally, they have not taken into account a sequential localization method in which multiple devices are localized one after another and the estimated positions of previous devices affect the localization of subsequent devices.

A. *Contributions*

The originality of the work presented here is mainly due to the originality of the problem of victims' localization using received data over multi-hop D2D-assisted emergency calls. Additionally, the Table III highlights the unresolved challenges in previous research and how they are addressed in this study. Moreover, the key contributions of this work are as follows:

- A new progressive propagation of multi-hop device positioning procedure that uses cumulative path information to locate multiple victims is proposed. Hence, a new algorithm called Multi-Victim Localization Algorithm

(*MVLA*) is proposed for the localization of multiple victim devices against the progression in time. Furthermore, three modes of *MVLA*, i.e., *MVLA*$_{\text{recent}}$, *MVLA*$_{\text{seq}}$, and *MVLA*$_{\text{all}}$, are proposed and evaluated under metrics such as localization error, delay, and algorithm complexity.

- The proposed localization method takes into account the assumptions that the absolute positions of relay devices are unknown and that the number of available reference nodes is minimal. Localization methods have not been previously studied incorporating these two assumptions.
- The proposed localization is performed under progressive increment in data. Hence, due to the lack of location data at the initial stage, a coarse positioning is proposed initially which enables the sizing and scheduling of rescue teams. This allows sending rescue teams to disaster areas before a more precise localization of the victims is available. This proposed procedure provides incremental localization with available data and with low latency (less than 3 minutes from the emergency call reception).
- The proposed localization algorithm is designed to generate zero additional control traffic. Although control signals are generally used to obtain data for localization, the proposed algorithm avoids the use of additional control messages for such data collection to avoid overloading the network traffic in out-of-coverage areas during an increase in emergency calls. LTE D2D interface-based outband D2D-assisted multi-hop protocols are utilized by smartphones to gather the localization data.
- A hybrid localization is proposed, which involves utilizing GPS, AoA, RSSI, and ToA data from emergency calls to determine the location of each device. Accuracy in such localization is shown to be higher compared to localizations with lesser measurements and standalone localization techniques. Also, as per our knowledge, the inequalities concerned with the AoA measurements with respect to different quadrants have not yet been discussed in the literature.
- The performance of the proposed localization modes is evaluated under various emergency scenarios. The proposed localization mode *MVLA*$_{\text{all}}$, is shown to be significant when compared with a competitive existing algorithm named RSSI-MonteCarlo boxed Localization (*RSSI-MCL*) in terms of localization error, end-to-end delay and number of functioning gNBs under extreme emergency scenarios. Furthermore, *MVLA*$_{\text{recent}}$ and *MVLA*$_{\text{seq}}$ is shown to be potential candidates to provide localization with reduced response delay under dense network areas with a trade-off of lower localization accuracy compared to *MVLA*$_{\text{all}}$

The remainder of this paper is organized as follows, In Section II, the proposed multiple victims' localization system is detailed, and the dynamic interval constraint problem is formulated. In Section III, the simulation results of the proposed localization algorithm are presented.

Table IV: The list of symbols and notations used in this paper

Symbol	Description
M	Set of emergency service enabled cellular devices
m_i	ith device in $m \in M$
(x_{m_i}, y_{m_i})	(x, y) the real coordinates of m_i
ϕ_i	GPS accuracy of the mobile m_i
α_{rssi}	Ratio of uncertainty on the RSSI distance measurement. The error margin is computed as the product of α_{rssi} and the predicted distance.
α_{AoA}	Error margin of AoA measurement
α_{toa}	Ratio of uncertainty on the ToA distance measurement. The error margin is computed as the product of α_{toa} and the predicted distance.
r_i	GPS accuracy radius of mobile m_i
R_{min}	Minimum of GPS estimation radius
R_{max}	Maximum of GPS estimation radius
GPS_i^x, GPS_i^y	GPS coordinates provided by m_i
$RSSI(m_i, m_j)$	RSSI of m_i estimated by m_j
$\Theta(m_i, m_j)$	AoA of m_i as estimated by m_j
$ToA(m_i, m_j)$	ToA of m_i as estimated by m_j
$d_{rssi}(m_i, m_j)$	RSSI assisted m_i to m_j distance estimation
$d_{toa}(m_i, m_j)$	ToA assisted m_i to m_j distance estimation
$\Theta(m_i, m_j)$	AoA estimation of signals provided by m_i to m_j
$P(m_i)$	Priority value of m_i
C_{m_i}	Emergency call initiated by m_i
$P_{C_{m_i}}$	Propagation path of C_{m_i}

II. Victims localization problem under partially nonoperational 5G network

A. System overview

Consider a network area in which $m \in M$ is a set of emergency service-enabled cellular devices whose location coordinates (x_m, y_m) are unknown. In this network, there is a set of operational base stations, represented as *gNB* $\in G$, whose positions are known. In the event of an emergency, a call is made from a device m, which employs a multi-hop protocol to forward the call to the network infrastructure as shown in Figure 1. Further, m incorporates its GPS location into the data it transmits to neighboring devices. These neighboring devices then add their own GPS information and measurements obtained from the signals they received from the transmitting device, including RSSI, AoA, and ToA.

Furthermore, this process of adding data and forwarding it to the next device is repeated through multiple hops until it reaches the emergency platform. Each device involved in the multi-hop transmission includes its own device ID and call ID in the data it transmits. Upon receiving the emergency call transmission, the emergency platform can decode the data and determine the number of participating devices by analyzing the unique device IDs associated with a specific Call ID. The platform then employs the location information gathered by each device and a Multi Victim Localization Algorithm (*MVLA*) to determine the location of the emergency device and update it to the rescue teams. The *MVLA* consists of several steps including constraint generation, dynamic localization mode selection, constraint linearization, and constraint satisfaction to determine the location of devices. Figure 3 illustrates the overall working scheme of the emergency localization service.

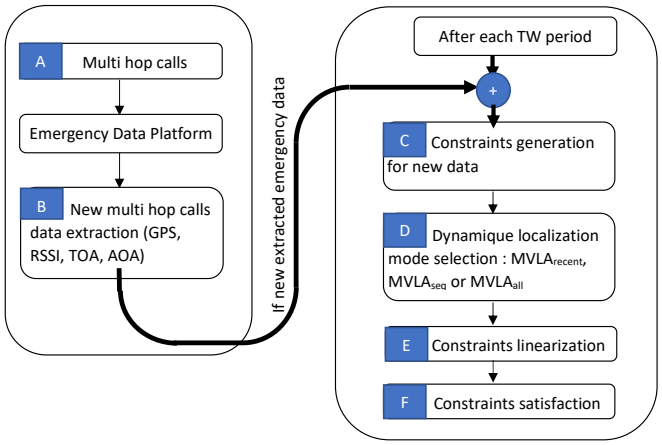

Figure 3: Emergency localization service working scheme.

B. Multi-hop data extraction

Once an emergency call, represented as C_{m_0}, is initiated, it follows a specific path, $P_{C_{m_0}} =< m_0, m_1, ..., m_k, gNB >$, where $m_0 \in M$ is the device that initiates the call, $m_1, ..., m_k$ are the devices the call passes through before reaching *gNB*. Once the emergency call is received by the emergency platform, the radio measurements inserted by the devices in the path are extracted. The RSSI of the device m_i as computed by its successor m_j in the path $P_{C_{m_0}}$ is represented as $RSSI(m_i, m_j)$. The GPS coordinates provided by the device m_i are represented as $GPS(m_i)$. The AoA of m_i as estimated by its successor m_j is represented as $AoA(m_i, m_j)$. The ToA of m_i as computed by *gNB* is represented as $ToA(m_i, gNB)$.

C. Constraints generation

The extracted data $RSSI(m_i)$, $GPS(m_i)$, $AoA(m_i, m_j)$ and $ToA(m_k, gNB)$, are converted into constraints by the emergency platform localization system.

1) GPS constraint: Each $GPS(m_i)$ data is converted into a constraint on the coordinates of the device m_i. The real position of the device m_i, (x_{m_i},y_{m_i}), is assumed to be within a given range (r_i) around the coordinates provided by $GPS(m_i)$, i.e., $(x_{GPS(m_i)}, y_{GPS(m_i)})$. More formally, the GPS constraint is written as:

$$\sqrt{\left(x_{m_i} - x_{GPS(m_i)}\right)^2 + \left(y_{m_i} - y_{GPS(m_i)}\right)^2} \leq r_i. \quad (1)$$

This constraint states that the actual location of device m_i is within a circular region, with the GPS coordinates of the device $(x_{GPS(m_i)}, y_{GPS(m_i)})$, as its center and a radius of r_i. The r_i, is determined by the minimum and maximum GPS radius bounds, R_{max}, and R_{min}, and is calculated based on the location accuracy of the GPS data for the device m_i given by ϕ_i. The ϕ_i is a value between 0.1 and 1, where a higher value corresponds to a more accurate GPS reading and, therefore, a smaller r_i. Next, r_i used in (1) is defined as $r_i = \frac{a}{b^{\phi_i}}$, where a and b are constants that assume that r_i varies exponentially with respect to ϕ_i. The minimum and maximum bounds for r_i, R_{max} and R_{min}, are determined by relating ϕ_i values of 0.1 and 1 to their corresponding r_i values. The minimum value of r_i, R_{min}, is defined as, $R_{min} = \frac{a}{b^1}$. The maximum value of r_i, R_{max}, is defined as, $R_{max} = \frac{a}{b^{0.1}}$. The values of a and b can be determined once the minimum and maximum limits of r_i, represented by R_{min} and R_{max}, are established through practical experiments and prior assumptions that take into account the specific scenario.

2) RSSI constraint: The RSSI data between two devices, m_i and m_j, is converted into two constraints on the distance between them. The equation (2) expresses the lower bound and equation (3) expresses the upper bound of the distance. Thereby, the RSSI constraint is given as:

$$\sqrt{\left(x_{m_i} - x_{m_j}\right)^2 + \left(y_{m_i} - y_{m_j}\right)^2} \geq d_{rssi}(m_i, m_j)(1 - \alpha_{rssi}), \quad (2)$$

$$\sqrt{\left(x_{m_i} - x_{m_j}\right)^2 + \left(y_{m_i} - y_{m_j}\right)^2} \leq d_{rssi}(m_i, m_j)(1 + \alpha_{rssi}), \quad (3)$$

where α_{rssi} denotes the ratio of uncertainty on the RSSI distance measurement. Moreover, the distance is estimated using the reverse log-distance path loss model, as given in $d_{rssi}(m_i, m_j) = d_0 \times 10^{\left(\frac{P_0 - P_r}{10 \times n_p}\right)}$, where p_r, p_0, and n_p are respectively, the measured RSSI power, the nominal transmission signal power of a cellular device received at a reference distance d_0, and the path loss exponent. The d_0 is usually taken as 1 m and n_p is determined based on the environment [41]. This model is more accurate than the free space path loss model in densely populated areas as it incorporates the impact of non-line-of-sight path loss [61].

3) AoA constraint: The estimated orientation of device m_i relatively to m_j, is denoted $AoA(m_i, m_j)$ and is converted into the following two constraints:

$$\theta_{m_i,m_j} \leq AoA(m_i, m_j) + \alpha_{AoA}, \quad (4)$$

$$\theta_{m_i,m_j} \geq AoA(m_i, m_j) - \alpha_{AoA}, \quad (5)$$

where α_{AoA} represents the error margin of the estimated AoA. The angles are measured at m_j in the anti-clockwise direction from the East. θ_{m_i,m_j} represents the actual orientation angle of m_i relatively to m_j.

Note that the area described by constraints (4) and (5) represents an angular sector. Using the coordinates of the devices, the constraints (4) and (5) are converted to the three cases defined in (6a), (6b), and (6c). These three cases are illustrated, respectively, by the examples (a), (b) and (c) of Figure 4. The first sub-figure relates to the case where $AoA(m_i, m_j)$ is close to 0 and $AoA(m_i, m_j) - \alpha_{AoA}$ becomes negative. The second case occurs when $AoA(m_i, m_j)$ is close to 2π and $AoA(m_i, m_j) + \alpha_{AoA}$ exceeds 2π. The third case concerns all the other situations. The angles are measured in radians and represent the angle formed by the vectors $\overrightarrow{West - East}$

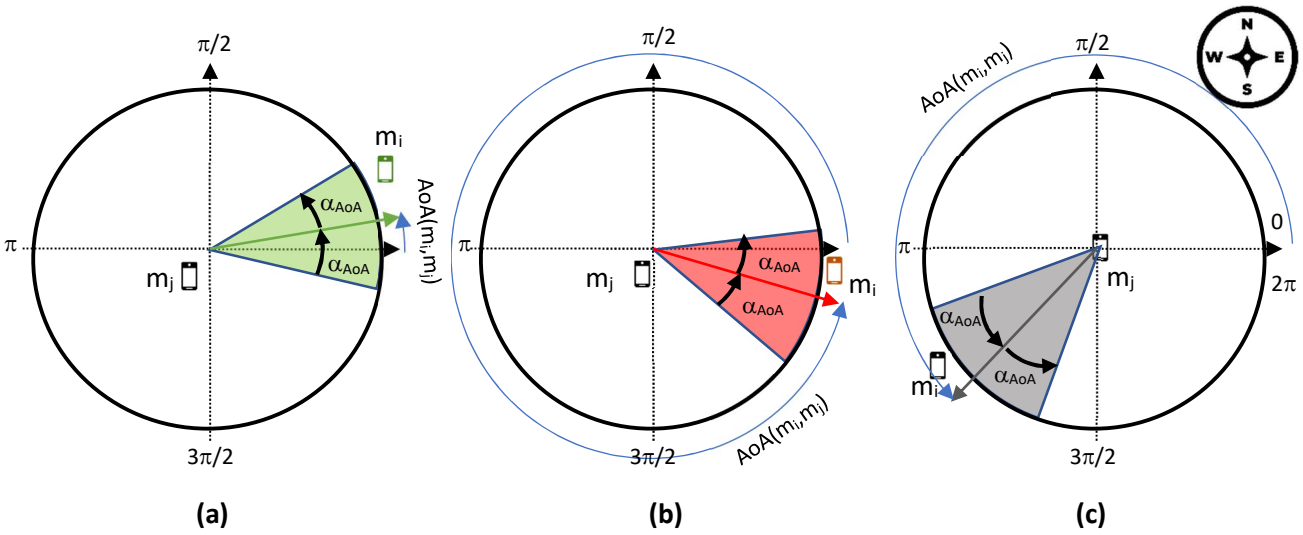

Figure 4: Three cases of the conversion of the estimated angle of arrival of the signal received by m_j from m_i, $AoA(m_i, mj)$, into constraints linking the coordinates (x_{mi}, y_{mi}) of m_i and (x_{mj}, y_{mj}) of m_j. The angle of arrival is a value between 0 and 2π measured in the counterclockwise direction starting from the East. The mobile icon shows the real position of the mobile m_i, while the $AoA(m_i, m_j)$ indicates the estimation computed by m_j of the orientation of m_i. The colored sectors depict the potential position of m_i according to the estimated angle $AoA(m_i, m_j)$. This area is computed using the estimated angle of arrival $AoA(m_i, mj)$ and the error margin of the AoA technique, α_{AoA}.

and $\overrightarrow{m_j m_i}$. The angle is measured in the counterclockwise direction and returns a value between 0 and 2π.

$$\begin{aligned}
&\text{if } \text{AoA}(m_i, m_j) - \alpha_{\text{AoA}} < 0 : \\
&\quad x_{m_i} - x_{m_j} > 0, \\
&\quad y_{m_i} - y_{m_j} < \sin(\text{AoA}(m_i, m_j) + \alpha_{\text{AoA}}).d(m_i, m_j), \\
&\quad y_{m_i} - y_{m_j} > \sin(\text{AoA}(m_i, m_j) - \alpha_{\text{AoA}} + 2\pi).d(m_i, m_j),
\end{aligned} \tag{6a}$$

$$\begin{aligned}
&\text{else if } \text{AoA}(m_i, m_j) + \alpha_{\text{AoA}} > 2\pi : \\
&\quad x_{m_i} - x_{m_j} > 0, \\
&\quad y_{m_i} - y_{m_j} < \sin(\text{AoA}(m_i, m_j) + \alpha_{\text{AoA}} - 2\pi).d(m_i, m_j), \\
&\quad y_{m_i} - y_{m_j} > \sin(\text{AoA}(m_i, m_j) - \alpha_{\text{AoA}}).d(m_i, m_j),
\end{aligned} \tag{6b}$$

$$\begin{aligned}
&\text{else :} \\
&\quad \arctan(x_{m_i} - x_{m_j}, y_{m_i} - y_{m_j}) \geq \text{AoA}(m_i, m_j) - \alpha_{\text{AoA}}, \\
&\quad \arctan(x_{m_i} - x_{m_j}, y_{m_i} - y_{m_j}) \leq \text{AoA}(m_i, m_j) + \alpha_{\text{AoA}},
\end{aligned} \tag{6c}$$

where $d(m_i, m_j) = \sqrt{(x_{m_i} - x_{m_j})^2 + (y_{m_i} - y_{m_j})^2}$.

4) ToA constraint: The connection between the final cellular phone in the multi-hop, m_k, and *gNB* is a typical 5G duplex communication. As a result, before forwarding the received call to the emergency platform, the *gNB* includes the information, $ToA(m_k, gNB)$, which represents the time difference between the transmission of the message from m_k and its reception at *gNB*. Thus, $ToA(m_k, gNB)$ can be converted into an estimation of the distance between m_k and *gNB* by using as $d_{toa}(ToA(m_k, gNB)) = ToA(m_k, gNB) \times 3 \times 10^8$.

Emergency service platform converts $ToA(m_k, gNB)$ data into two constraints:

$$\sqrt{(x_{m_k} - x_{gNB})^2 + (y_{m_k} - y_{gNB})^2} \geq d_{toa}(m_k, gNB)(1 - \alpha_{toa}), \tag{6}$$

$$\sqrt{(x_{m_k} - x_{gNB})^2 + (y_{m_k} - y_{gNB})^2} \leq d_{toa}(m_k, gNB)(1 + \alpha_{toa}), \tag{7}$$

where α_{toa} is the ratio of uncertainty on the ToA based distance measurement. Moreover, as the distance between a transmitting device (m_i) and a receiving device (m_j) gets larger, the values of α_{toa} and α_{rssi} will also increase as the error in distance estimation increases. Additionally, after a list of constraints for a particular device is compiled, it is combined to calculate the potential location of the device. An example of this process can be seen in Figure 5, which shows how a constraint satisfaction algorithm can be used to find the location of a device when GPS, RSSI, ToA, and AoA measurements are available.

D. Dynamic localization mode selection

In this section, the proposed multi-victim localization algorithm and its working scheme is presented. This algorithm extracts radio data such as RSSI, GPS, AoA, ToA from emergency calls and generate constraints as explained in the Sections II-B and II-C. Such constraint generation is done during each time interval of *TW* and localization results are given at the end of *TW*. Thus, during each *TW*, a Dynamic Constraint Satisfaction Problem (DCSP) is formed which corresponds to a varying set of constraints on devices' coordinates. Further, the set of constraints used in the DCSP is dependent on the

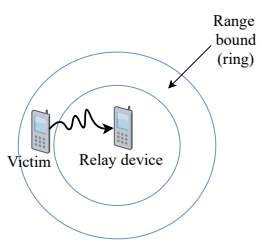

(a) Range constraint: using RSSI or ToA.

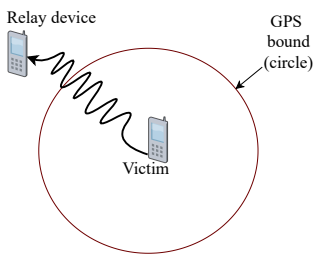

(b) GPS measure constraint.

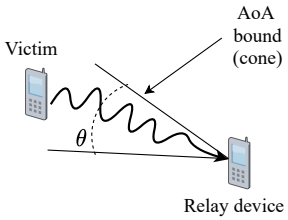

(c) Angle constraint: using the Angle of Arrival (AoA).

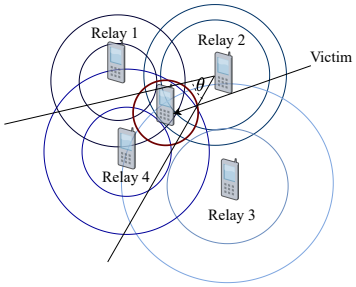

Figure 5: Victim localization with GPS, AoA and n range measurements (e.g., RSSI, ToA).

chosen mode of the Multiple Victims' Localization Algorithm (*MVLA*). Such *MVLA* modes are as follows:

- $MVLA_{recent}$: Only the most recent data received during the past time window, *TW*, is taken into account. Data from previous emergency calls are ignored and only the sources of the calls received during the last *TW* period are localized.
- $MVLA_{seq}$: Instead of ignoring the received data before *TW*, the result of previous DCSP resolutions is added to the list of newly generated constraints. The previous DCSP resolutions are denoted for a device m_i as $x_{m_i} \leq x_{max_i}; x_{m_i} \geq x_{min_i}$ and $y_{m_i} \leq y_{max_i}; y_{m_i} \geq y_{min_i}$.
- $MVLA_{all}$: In each *TW*, the entire problem, including all previously generated constraints and the latest ones, is considered in the DCSP.

Furthermore, the order in which devices are to be localized during a certain time interval is done based on a priority ordering mechanism. Thereby, the cellular devices participating in each multi-hop call are ordered based on a priority value, $P(m_i)$, assigned to each device. Further, the devices involved in a multi-hop call are localized in decreasing order of priority. This priority value is determined using the following equation:

$$P(m_i) = w_{\phi_i}.\phi_i + w_{\frac{1}{d_{gNB_i}}}.\frac{1}{d_{gNB_i}} + w_{NC_i}.NC_i, \quad (8)$$

where $\phi_i \in [0.1, 1]$ represents the estimated GPS accuracy provided by the mobile device m_i (see Section II-C1). d_{gNB_i} corresponds to the distance between m_i and its nearest *gNB*. Further, NC_i signifies the number of received calls by m_i, where m_i has served as either the source or a relay device. Moreover, d_{gNB_i} is calculated based on the *gNB* coordinates (x_{gNB}, y_{gNB}) and the GPS coordinates of the device ($x_{GPS(m_i)}$,$y_{GPS(m_i)}$). The factors ϕ_i, $\frac{1}{d_{gNB_i}}$ and NC_i were chosen as they can determine the localization accuracy of a device. The weights of these three factors given by w_{ϕ_i}, $w_{\frac{1}{d_{gNB_i}}}$, w_{NC_i} were set to 3, 5, 1 respectively. Moreover, the weights of the factors, ϕ_i, $\frac{1}{d_{gNB_i}}$ and NC_i, were set according to the significance of each technique ($\frac{1}{d_{gNB}}$ being the most significant, ϕ the second, and NC being the least significant). Note that to gain a better understanding of how each weight value affects the algorithm's performance, it is essential to conduct further research and analysis. It was assumed that $\frac{1}{d_{gNB}}$ is the most significant factor since the gNB provides localization information by taking the combination of both the cellular and satellite signal measurements. Relegated to second place, it was assumed that the GPS technique provides accurate localization when the conditions are favorable (number and visibility of the satellites). Finally, *NC* was given the least weight since the reliability of the location estimation derived from the received calls can be volatile over time.

E. Constraints linearization

After completing the priority ordering step, the selection of constraints to be satisfied in order to localize the victim device is done based on the *MVLA* mode. Next, the non-linear constraints in the selected constraint set are transformed into a set of linear constraints using the Successive Linear Programming (SLP) algorithm [62]. Figure 6 illustrates the victim localization process using the SLP assisted constraint satisfaction method [62].

This algorithm transforms each non-linear constraint into a group of linear constraints that approximate the region where the constraints are satisfied. The transformation is achieved through the use of a first-order Taylor series approximation. For example, the GPS constraint in (1) is converted to four

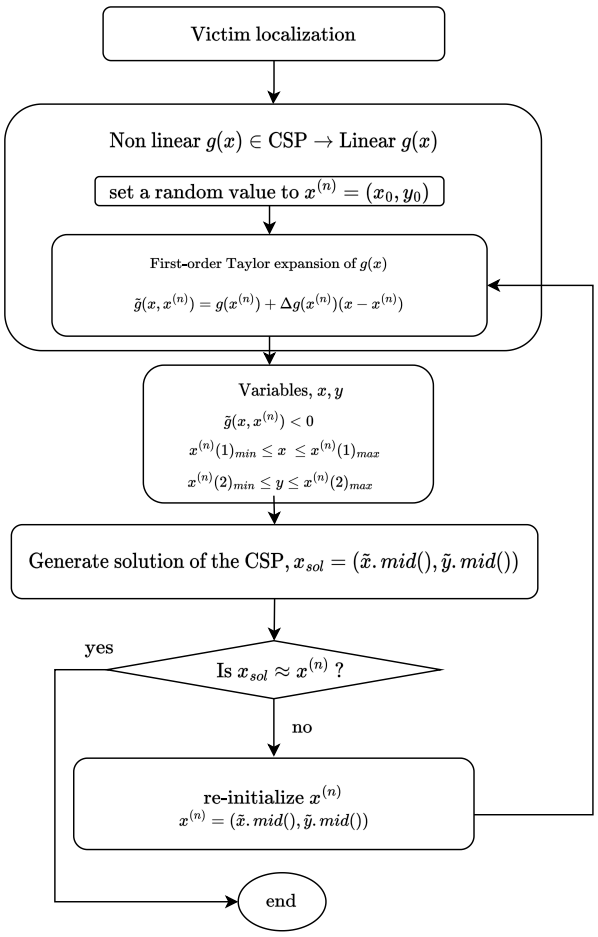

Figure 6: Victim Localization Procedure based on a Successive Linear Programming (SLP) and Constraint Satisfaction approach.

linear constraints of the form:

$$x_{m_i} \geq x_{GPS(m_i)} - r_i, \tag{9a}$$
$$x_{m_i} \leq x_{GPS(m_i)} + r_i, \tag{9b}$$
$$y_{m_i} \geq y_{GPS(m_i)} - r_i, \tag{9c}$$
$$y_{m_i} \leq y_{GPS(m_i)} + r_i. \tag{9d}$$

The RSSI constraint in the form (2) and (3) is transformed into five linear constraints as (10a), (10b), (10c), (10d), (11e). In the case of ToA constraints, its approximation can be performed in a similar manner as the RSSI constraints.

$$x_{m_i} \leq x_{m_j} + d_{rssi}(m_i, m_j)(1 + \alpha_{rssi}), \tag{10a}$$
$$x_{m_i} \geq x_{m_j} - d_{rssi}(m_i, m_j)(1 + \alpha_{rssi}), \tag{10b}$$
$$y_{m_i} \leq x_{m_j} + d_{rssi}(m_i, m_j)(1 + \alpha_{rssi}), \tag{10c}$$
$$y_{m_i} \geq x_{m_j} - d_{rssi}(m_i, m_j)(1 + \alpha_{rssi}), \tag{10d}$$

$$\begin{aligned} x_{m_i} &\geq x_{m_j} + d_{rssi}(m_i, m_j)(1 - \alpha_{rssi})cos(\pi/4) \vee \\ x_{m_i} &\leq x_{m_j} - d_{rssi}(m_i, m_j)(1 - \alpha_{rssi})cos(\pi/4) \vee \\ y_{m_i} &\geq y_{m_j} + d_{rssi}(m_i, m_j)(1 - \alpha_{rssi})sin(\pi/4) \vee \\ y_{m_i} &\leq y_{m_j} - d_{rssi}(m_i, m_j)(1 - \alpha_{rssi})sin(\pi/4). \end{aligned} \tag{11e}$$

In addition, when AoA constraints are present, the AoA constraint expressed as $AoA(m_i, m_j) - \alpha_{AoA} \leq tan^{-1}(y_{m_i} - y_{m_j}, x_{m_i} - x_{m_j}) \leq AoA(m_i, m_j) + \alpha_{AoA}$ in (6a) is converted into two linear constraints:

$$\begin{aligned} &(x_{m_j} - x_{m_i})cos(AoA(m_i, m_j) - \alpha_{AoA}) \\ &+(y_{m_j} - y_{m_i})sin(AoA(m_i, m_j) - \alpha_{AoA}) \geq 0, \end{aligned} \tag{12a}$$

$$\begin{aligned} &(x_{m_j} - x_{m_i})cos(AoA(m_i, m_j) + \alpha_{AoA}) \\ &+(y_{m_j} - y_{m_i})sin(AoA(m_i, m_j) + \alpha_{AoA}) \leq 0. \end{aligned} \tag{12b}$$

Figure 7 schematizes the effect of the linearization of constraints. The figure shows that constraint linearization causes a relaxation of the initial constraint leading to the enlargement of the feasible area (set of positions that satisfy the constraint). However, no feasible solution is excluded by the constraints' conversion. Figure 7 also shows that AoA conversion keeps the feasible area intact without any relaxation.

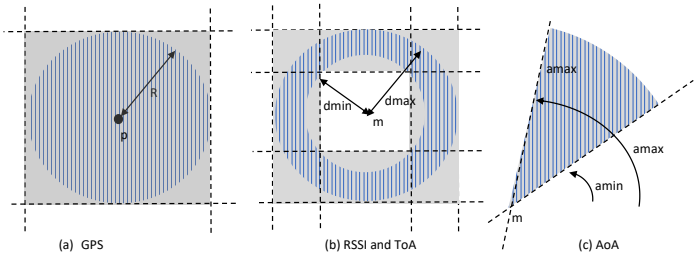

Figure 7: Conversion scheme of the non-linear constraints. The hatched area represents the initial feasible area, dotted lines represent the linear constraints obtained after the conversion, and the gray area represents the approximated feasible area obtained by the relaxation.

F. Constraints satisfaction

The batch of linear inequalities generated with regard to the list of devices in received calls is solved using an SLP-assisted DCSP. Algorithm 1 gives how the constraints are prepared for the DCSP that works every *TW* cycle. The Algorithm 1 requires the following inputs: the list of devices in the received calls (Dev), the new constraints generated by the recent calls (*new_Cst*), previously generated constraints (*old_Cst*), previously estimated bounds for devices' locations (*slv_Cst*), and the selected dynamic localization mode, *MODE*. If the $MVLA_{recent}$ mode is selected, the constraints which are generated using the received calls in the last *TW* period are considered for localization. Next, if the mode is $MVLA_{all}$, the total constraints generated until the current *TW* are considered for localization. Next, if the mode is set to $MVLA_{seq}$, the current location bounds of the devices are updated using constraints generated from the received calls in the last *TW* period, and any previous *slv_Cst* available. Further, such a DCSP is continued for a certain number of iterations until the solution for the victim localization is converged to a fixed point as given in Figure 6. The converged solutions provide the locations of the devices considered for localization.

Algorithm 1: Cyclical procedure of victim localization service.

Inputs: *Dev*; *new_Cst*; *old_Cst*; *slv_Cst*; *MODE*
Outputs: *slv_Cst*
Dev=*Dev* $\bigcup$ extractDevices(*new_Cst*)
Compute the priority of $d \in$ *Dev*
if *MODE*==$MVLA_{recent}$ **then**
  slv_Cst=*slv_Cst* $\bigcup$ SLP(*new_Cst*)
end
if *MODE*==$MVLA_{all}$ **then**
  slv_Cst=*slv_Cst*$\bigcup$ SLP(*new_Cst*, *old_Cst*)
end
if *MODE*==$MVLA_{seq}$ **then**
  slv_Cst=*slv_Cst*$\bigcup$ SLP(*new_Cst*, *slv_Cst*)
end
return *slv_Cst*

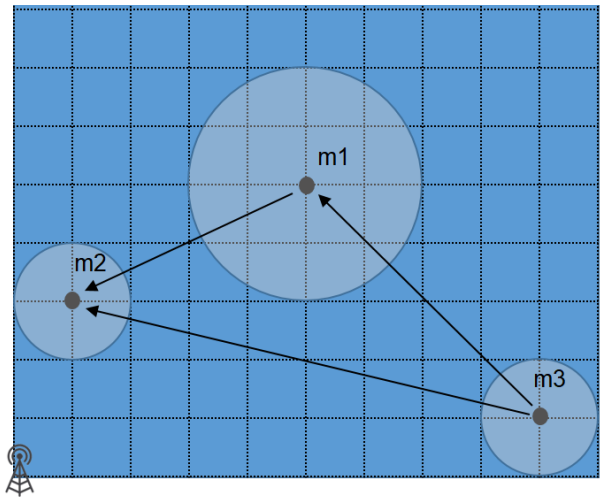

Figure 8: Example with three cellular phones m_1, m_2, m_3. The victim m_3 sends an emergency call that follows two paths. The depicted positions of the phones correspond to the provided GPS positions. The circle around the position depicts the GPS accuracy.

Additionally, to illustrate the process of device localization using the proposed methods, one example is provided using the $MVLA_{recent}$. Consider an example scenario involving three cellular phones m_1, m_2, and m_3 with computed priorities of 10, 12, and 8 respectively. In this scenario, it is assumed that m_1, m_2, and m_3 are located at coordinates (5, 5), (1, 3), and (10, 0) respectively, and their r_i values are 1, 2, and 1. The calls from these devices are received by the only functional gNB located at (0, 0).

Consider the case where the emergency service receives two emergency calls from the same original caller m_3. The first call follows the path $< m_3, m_1, m_2, gNB >$ and the second call follows the path $< m_3, m_2, gNB >$. This example is illustrated in Figure 8. The GPS and RSSI measurements included in the two received calls are used to generate constraints that give the following inequalities:

$$
\begin{aligned}
&1)\ \sqrt{(x_{m_3}-10)^2+(y_{m_3}-0)^2} \le 1,\\
&2)\ \sqrt{(x_{m_1}-5)^2+(y_{m_1}-5)^2} \le 2,\\
&3)\ \sqrt{(x_{m_2}-1)^2+(y_{m_2}-3)^2} \le 1,\\
&4)\ 4 \le \sqrt{(x_{m_1}-x_{m_3})^2+(y_{m_1}-y_{m_3})^2} \le 7,\\
&5)\ 3 \le \sqrt{(x_{m_2}-x_{m_1})^2+(y_{m_2}-y_{m_1})^2} \le 5,\\
&6)\ 7 \le \sqrt{(x_{m_2}-x_{m_3})^2+(y_{m_2}-y_{m_3})^2} \le 10.
\end{aligned}
\tag{11}
$$

The process of locating the victim starts with the highest priority cellular phone, m_2. In the first step, only the constraints related to a single phone (Constraints 1, 2, and 3) and those involving m_2 are considered. The non-linear constraints in 1, 2, 3, 5, and 6 are transformed into linear constraints, as outlined in Section II-E. Next, the localization of m_2 is achieved using the DCSP method. The method produces results by confining the x coordinate to within the range of [0.015, 2] and the y coordinate to within [2.27, 3.67]. The positions of the remaining devices are then estimated using the localized m_2. Moreover, the expected location of m_2 given by (12) is added to the inequalities system:

$$
\begin{aligned}
&7)\ 0.015 \le x_{m_2} \le 2,\\
&8)\ 2.27 \le y_{m_2} \le 3.67.
\end{aligned}
\tag{12}
$$

Subsequently, the constraints involving m_1 and the constraints related to a single cellular phone (Constraints 1, 2, 3, 4, 5, 7, 8) are resolved, resulting in the localization of the x coordinate of m_1 within the range [3.53, 5.39] and the y coordinate within [3.49, 6.37] as given in (13).

$$
\begin{aligned}
&9)\ 3.53 \le x_{m_1} \le 5.39,\\
&10)\ 3.49 \le y_{m_1} \le 6.37.
\end{aligned}
\tag{13}
$$

The predicted bounds of m_1 are then added to the inequalities system to locate the final cellular phone, m_3. By solving the inequalities system that encompasses constraints 1, 2, 3, 4, 6, 7, 8, 9, and 10, m_3 is localized with its x coordinate in the range [9.3, 10.66] and y coordinate in [1.96, 2]. Moreover, if the selected localization mode is $MVLA_{seq}$, the estimated positions of m_1, and m_2, and m_3 will be used as constraints in the next localization cycle. In contrast, $MVLA_{all}$ takes into account all received constraints and determines the location of the unknown device.

III. Performance Analysis

The simulation environment comprised two key components: the first part involved in the reception of emergency calls from out-of-coverage areas to the 4/5G network using M-HELP [14] protocol, while the second part involved extracting data from the received emergency calls to determine the location of victims. The simulation considered a 4/5G network with a suburban area of 16.2×21 km^2 and 15,000 cellular

devices, with only 7 out of 39 gNBs functioning after a disaster. The total cellular devices are uniformly distributed in the network area and the number of emergency devices are varied from 100 to 3000. Out of the total number of devices, 25% of them are in-coverage devices. Note that any device in the network can function as an emergency, a relay, or an idle device at any given time. Furthermore, the distribution of the in-coverage or out-coverage devices in the network area is depicted in Figure 9a. The three scenarios in Figure 9 are used to denote different gNB distributions in the network area. Moreover, in these scenarios, the emergency devices are randomly distributed over the network area to denote complex localization cases where the emergency devices are dispersed over the network area. In disperse scenario, the CSP needs to localize the disperse devices with separate bounds whereas the localization of clustered emergency devices is less complex and possible with a unified bound. Additional details on the network and M-HELP parameters are outlined in Table V. The network simulation was done using AnyLogic software, while the emergency center simulation was implemented using the Tubex Python library [63] and executed on the Google Colab platform [64]. The devices were localized using three different modes: $MVLA_{all}, MVLA_{recent}$, and $MVLA_{seq}$.

The uncertainty parameters for each measurement type are expressed in Table VI. The possible range of r_i, can vary from a few meters to several tens of meters in ideal conditions. However, it can drop to several tens or even hundreds of meters in challenging situations such as disasters. The R_{min}, and R_{max} were determined as given in Table VI. This is based on practical experiments that demonstrate an average minimum GPS accuracy of 2 m. Moreover, the R_{max} is set to 1000 m, considering worst-case scenarios of GPS accuracy during a scenario with no line of sight view of the satellites. Furthermore, in our scenarios, it was taken into account that the devices have various techniques with varying degrees of accuracy, and the accuracy level reflects the precision of each technique. For example, when the AoA is measured, the resulting estimate of the angle will have a specific level of precision. We assume that this precision falls within the previously established limits for the system, based on past practical experiments conducted in this area.

The accuracy of RSSI, ToA, and AoA measurements were determined through experiments evaluating their precision for localization. Data from these experiments showed the minimum and maximum error margins for each measurement type in different environments, allowing for calculating the error of a target node. AoA measurement is found to have a total error range of $\pi/18 - \pi/3$ [22], [23], and in this study, its error margin is estimated as $\pi/6$ on each side of the central axis. The accuracy of RSSI distance estimation can be affected by various factors such as wireless channel conditions, interference, noise, and frequency band. It is estimated to fluctuate by up to 80% in a chaotic disaster environment. ToA-based distance estimation, on the other hand, is expected to have an error margin of 20%, since ToA is considered for devices under coverage. The values for accuracy parameters are given in Table VI.

Table V: Sub-urban area emergency simulation parameters.

Parameter	Value
w_{ϕ_i}	3
$w_{\frac{1}{d_{gNB_i}}}$	5
w_{NC_i}	1
Update time interval, TW	120 sec
Total network area	16.2×21 km^2
gNB coverage	1.5 km
Total gNB number	39
Amount of working gNBs	7
Amount of broken gNBs	32
Total UE spread	RAND (16.2,21)
Total Emergency UE spread	RAND (16.2,21)
Total Simulation running time	45 minutes

A. *Performance study of MVLA algorithms*

The proposed *MVLA* modes are evaluated and compared to an existing *RSSI-MCL* scheme proposed in [43] using three metrics: Average Distance Error (ADE), computing delay, and algorithm complexity. ADE denotes the difference between the real position, $x_{r_{m_i}}, y_{r_{m_i}}$, and the estimated position, $x_{e_{m_i}}, y_{e_{m_i}}$ of a given cellular phone m_i given as $ADE = \frac{\sum_{i=1}^{n} \sqrt{\left(x_{e_{m_i}} - x_{r_{m_i}}\right)^2 + \left(y_{e_{m_i}} - y_{r_{m_i}}\right)^2}}{n}$, where n is the total number of localized victims. Moreover, computing delay is the time difference between receiving emergency data and updating the estimated victim location bounds. Next, algorithm complexity (ϵ) is the computational burden of the algorithm in terms of the number of iterations run to compute the total victim locations given as $\epsilon = \frac{\eta_{iter}}{TW}$, where η_{iter} is the number of iterations runs per *TW*.

First, Figure 10a depicts the ADE obtained from various combinations of the radio measurements against the progression in time. The obtained results show that the approach with *GPS+RSSI+AoA+ToA* resulted in the greatest reduction of the localization error. Indeed, when the number of constraints increases, the localization area that satisfies all the constraints becomes smaller. It is noted that the localization error decreased rapidly in the initial stages, as the emergency calls came successively from nearby in-coverage locations. Over time, the ADE gradually increased due to the receipt of emergency calls from devices located at farther distances and hence longer paths. This is because the information about the farther devices is reduced. Eventually, the ADE stabilized as it became impossible to further converge the localization estimations of the devices.

Table VI: Parameters that define the error in each type of measurement.

Parameter	Value
Radius: GPS, R_{min}	2 m
Radius: GPS, R_{max}	1000 m
Range: RSSI, α_{RSSI}	0.8
Angle: AoA, α_{AoA}	$\pi/6$
Range: ToA (in-coverage), α_{ToA}	0.2

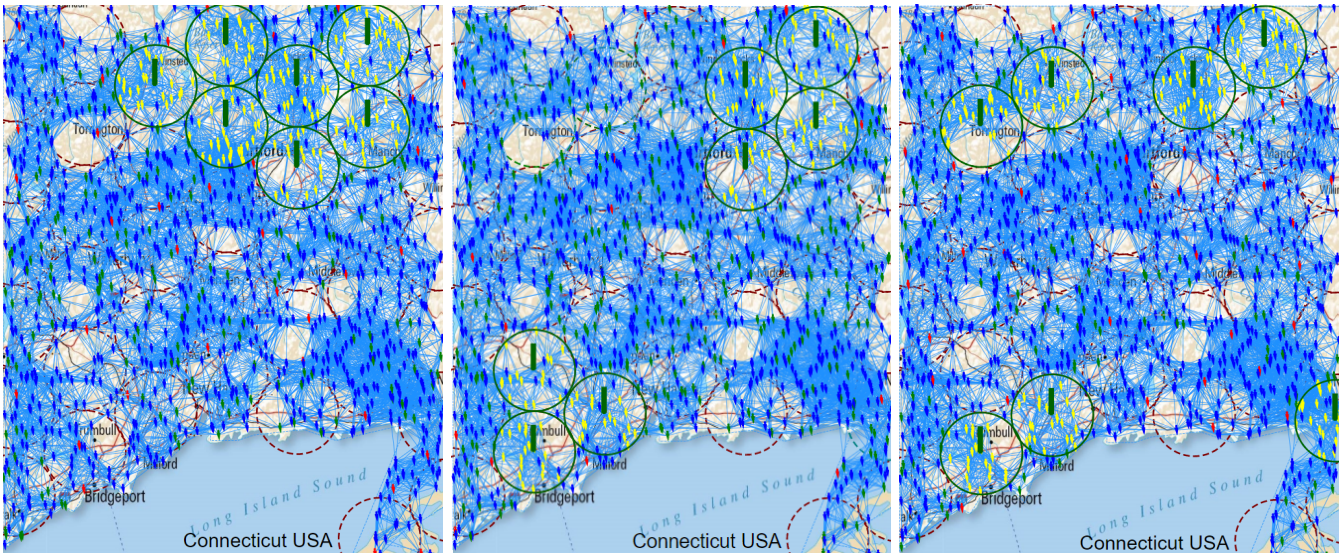

(a) Scenario 1: all operational gNBs are located in the same region.

(b) Scenario 2: operational gNBs are located in two different regions.

(c) Scenario 3: operational gNBs are located in four different regions.

Figure 9: Uniformly distributed 39 gNBs, with only 7 functioning, and 15,000 UEs in the AnyLogic® software. Linked UEs (resp. UE-to-gNB links) represent D2D (resp. traditional) communication possibilities. Dark green circles represent the functioning gNBs according to three scenarios. Non-functioning gNB coverage areas are indicated by red circles with dashes. Emergency devices, relay devices, in-coverage devices, and idle devices are represented respectively by the colors, red, green, yellow, and blue.

Figure 10b depicts a comparison in ADE between the three proposed modes $MVLA_{all}$, $MVLA_{seq}$, and $MVLA_{recent}$ under the progression in time. It is observed that $MVLA_{seq}$ and $MVLA_{recent}$ has a higher ADE than $MVLA_{all}$. This is attributed to the reduction in the number of constraints considered in each cycle by $MVLA_{seq}$ and $MVLA_{recent}$, which impacts their performance. These modes generate constraints using data collected within the previous *TW* interval. The rapid increase in the ADE in $MVLA_{seq}$ and $MVLA_{recent}$ over time is observed due to the limited data and hence fewer constraints generated for victim devices located at far off locations. However, $MVLA_{seq}$ performs slightly better than $MVLA_{recent}$ as it also took into account the previously estimated localization results in determining localization bounds of devices. Nevertheless, in situations where low complexity algorithms are needed, especially under large emergency data volumes, $MVLA_{seq}$ and $MVLA_{recent}$ modes serve as suitable alternatives to the $MVLA_{all}$ mode.

Figure 10c depicts the obtained ADE against the progression in time under the precision of the employed radio measurements: $\alpha_{rssi}, \alpha_{toa}$ and α_{AoA}. It is observed that the lowest ADE is achieved when measurements with higher precision are combined. An increase in precision leads to a smaller geographical area that meets the constraints as the accuracy of measurements is improved.

Figure 11 illustrates the resulting ADE under different distributions of functioning gNBs across the network area. Furthermore, The results indicate that when the functioning gNBs are concentrated in one corner of the network, the ADE is worse than in scenarios where the operational gNBs are scattered across the network area. In Scenarios 2 and 3 of Figures 9b and 9c, there is a higher availability of functioning gNBs in close proximity. Therefore the number of hops required to reach such a gNB decreases. This leads to a situation where emergency calls are routed through fewer intermediate relay devices. Hence the propagation of positioning uncertainty is reduced when gNBs are distributed as in Scenario 2 or even more as in Scenario 3. Conversely, the ADE is higher when gNBs are clustered together as in Scenario 1.

Figure 12a depicts the algorithm complexity against the progression in time. It is seen that the $MVLA_{all}$ has a higher complexity than $MVLA_{seq}$ and $MVLA_{ord}$, due to handling a larger number of constraints, as given by the Algorithm 1. Figure 12b depicts the computing delay of the *MVLA* modes under the progression in time. The computing delay of localization estimation is also influenced by the number of constraints handled by the localization mode. Thereby, it is seen that $MVLA_{all}$ has a higher delay than the two other modes. It is observed that $MVLA_{all}$ still maintains a fast response time of 1 second for a scenario with 340 victims and 15000 total devices. However, in scenarios with an increased number of victims and a denser cellular network, the response time is likely to be higher.

Next, the performance of $MVLA_{all}$ mode is compared with the method *RSSI-MCL* proposed by [43]. *RSSI-MCL* uses a combination of particle filtering and RSSI-based distance constraints to localize the nodes. For each cellular phone, m_i, the emergency service platform extracts the couples of data of the type $RSSI(m_j, m_i)$ and $GPS(m_j)$. Each couple of data $RSSI(m_j, m_i)$ and $GPS(m_j)$ is used to compute a box area $\Gamma(m_j, m_i)$ where m_i is expected to be (see Figure 13a). The intersections of all the $\Gamma(m_j, m_i)$ boxes for a given

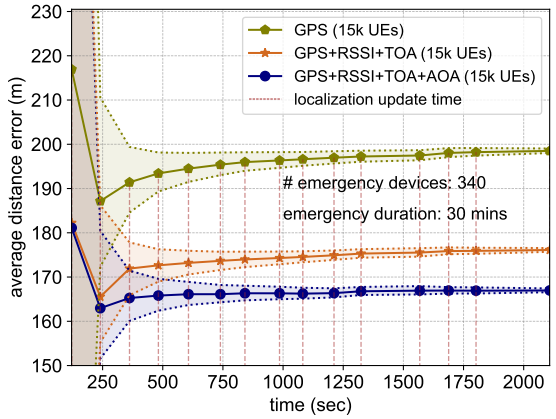

(a) Variation in ADE under *MVLA*$_{all}$ mode under different combinations of GPS, RSSI, ToA, and AoA.

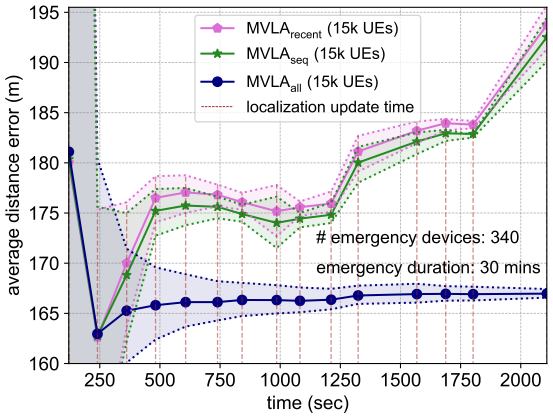

(b) Variation of ADE under *MVLA*$_{recent}$, *MVLA*$_{recent\text{-}seq}$ and *MVLA*$_{all}$. Localization scheme: GPS+RSSI+AoA+ToA.

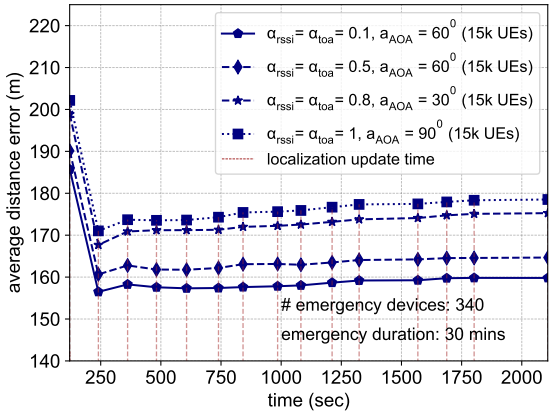

(c) Variation of ADE $\alpha_{RSSI}, \alpha_{ToA}, \alpha_{AoA}$ values in *MVLA*$_{all}$ mode. Localization scheme: GPS+RSSI+AoA+ToA.

Figure 10: Performance analysis of proposed *MVLA* modes under a varying number of radio measurements, constraint size, and error limits. The total number of emergency devices localized = 340, emergency calls occurring duration = 30 minutes. The minimum and maximum error limits of each combination are denoted by the upper and lower bounds of the filled region with its distinct color. The localization update time instances are indicated by periodic dashed brown vertical lines, occurring with each *TW*. gNB distribution as in Figure 9a.

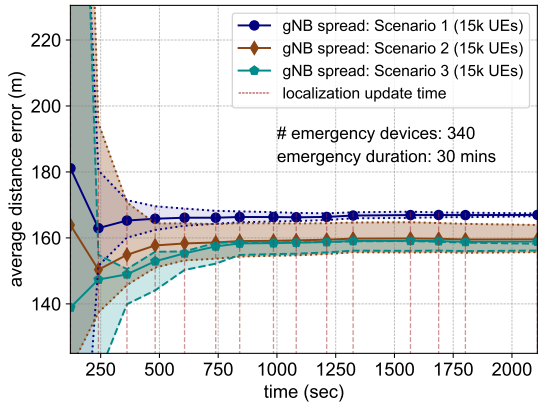

Figure 11: Impact of the functioning gNBs distribution over the average distance error (ADE) with *MVLA*$_{all}$ mode.

cellular phone, m_i, is called anchor box $\Gamma(m_i)$. Then 50 particles uniformly distributed in the anchor box $\Gamma(m_i)$ are generated. Ultimately, only the particles that meet the RSSI constraints are used to determine the target location. The mean of these particles is considered as the estimated position of m_i. Furthermore, in the scenarios depicted in the Figures 13b, 13c, 13d, the emergency devices are distributed randomly across the network area.

In Figure 13b, the ADE obtained using *MVLA*$_{all}$ and *RSSI-MCL* is presented. It is noted that the lower accuracy in *RSSI-MCL* is due to the utilization of smaller number of radio measurements than *MVLA*$_{all}$. Furthermore, the *RSSI-MCL* method fails to exploit the complete potential of the particle filtering method as it distributes particles uniformly over the anchor box when localizing static devices. Moreover, in contrast to *MVLA*$_{all}$, *RSSI-MCL* does not take into account

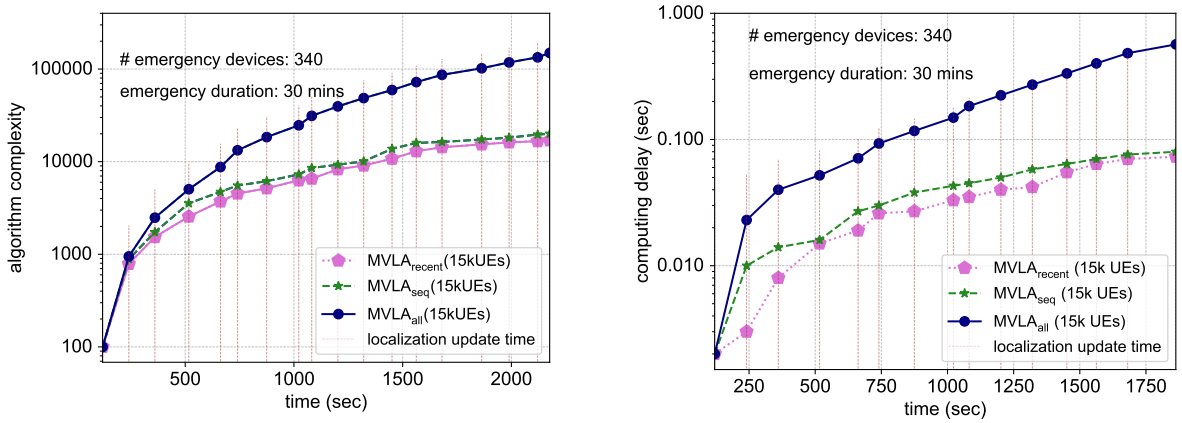

(a) Comparison of algorithm complexity against time.

(b) Comparison of computing delay against time.

Figure 12: Computational complexity and delay under the *MVLA*$_{recent}$, *MVLA*$_{recent\text{-}seq}$ and *MVLA*$_{all}$ schemes. Localization scheme used: GPS+RSSI+AoA+ToA. Parameters: R_{min} = 2 m, R_{max} = 1000 m, α_{RSSI} = 0.8, α_{ToA} = 0.2, α_{AoA} = 30^0. Total number of emergency devices localized = 340, emergency calls occurring duration = 30 minutes. gNB distribution as in Figure 9a.

the position uncertainty in relay devices, which is particularly relevant in emergency scenarios. The localization error of intermediate relay devices impacts significantly on the overall localization accuracy due to the propagation of localization along multi-hop devices. Next, it is noted that the accuracy in RSSI and GPS measurements can significantly deteriorate due to high levels of interference leading to inaccuracies. Additionally, GPS can introduce considerable errors when devices do not have direct Line of Sight (LOS) link with satellites. $MVLA_{all}$ method incorporates RSSI and GPS, but also AoA and ToA to reinforce the resultant localization accuracy. Thereby, $MVLA_{all}$ method has the potential to perform well in terms of accuracy during emergency situations. As a result, *MVLA*$_{all}$ demonstrates a reduction of ADE by 55.97% compared to *RSSI-MCL*.

Furthermore, the time response of *RSSI-MCL* and *MVLA*$_{all}$ according to the number of emergency devices is presented in Figure 13c. On average, *RSSI-MCL* took more time than *MVLA*$_{all}$. Indeed, the computation of the anchor boxes and extracting the particle positions that satisfy the constraints slowed down the *RSSI-MCL* method. Also, it is observed that in *MVLA*$_{all}$, the time response reaches 10 seconds when the number of victims is between 2000 to 3000 with 15000 available devices. The time response is expected to reach up to several minutes under large network scenarios (10^5 devices with 10^4 emergency calls). In such a case, the use of lighter modes, *MVLA*$_{seq}$ and *MVLA*$_{recent}$, is preferred.

Moreover, the impact of functioning gNBs on the ADE is seen in Figure 13d. The average localization estimation error declines with the increase in the number of functioning gNBs. The number of users under coverage increases and hence the location estimation accuracy in such devices increases. Hence, the sequential relay devices' location estimations are improved and victim location estimation accuracy is increased. The, *RSSI-MCL* has a lower decrement than *MVLA*$_{all}$ in localization error since it used lesser radio measurement types. In contrast, *MVLA*$_{all}$ uses the dynamic constraint satisfaction algorithm with the combination of four radio measurement types.

B. Devices' mobility and victims' localization

Mobility of both victims' and relay devices is an intrinsic characteristic in the victims' localization process. The mobility feature must be considered at the two stages of the disaster management process, i.e., the victims' assessment and the localization. During the victims' assessment stage, protocols such as M-HELP [14] or 5G-SOS [15] allow forwarding emergency calls to the safety service platform. Therefore, it is important to improve the emergency call relay protocols to automatically resend the localization-related data when the victim's location significantly changes compared to the last reported position.

In order to localize the victim, it's important to consider constraints related to the respective data reception time periods as the victim or relay devices involved are not in the same position. The satisfaction of these constraints may be then impossible since some constraints are outdated. Further, to allow the progressive consideration of the automatic resending of the emergency call when victims move, the localization procedure must be launched periodically and the recent constraints, generated from recently received emergency calls, should be prioritized against the previously extracted constraints. This prioritization may take the form of penalties or weights assigned to the constraints according to the freshness of the received data. The possible unfeasibility of the generated system leads to the adoption of a new optimization approach where the objective is to reduce the weighted sum of unsatisfied constraints rather than satisfying all the constraints. To tackle this scenario, various techniques such as Meta-heuristics [65] (Genetic Algorithms, Simulated Annealing,

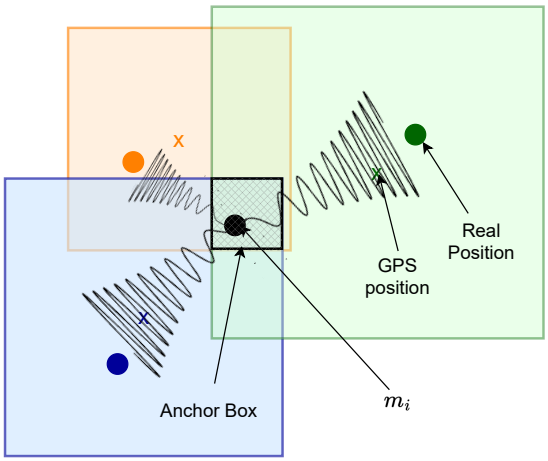

(a) Anchor box computation in *RSSI-MCL* method.

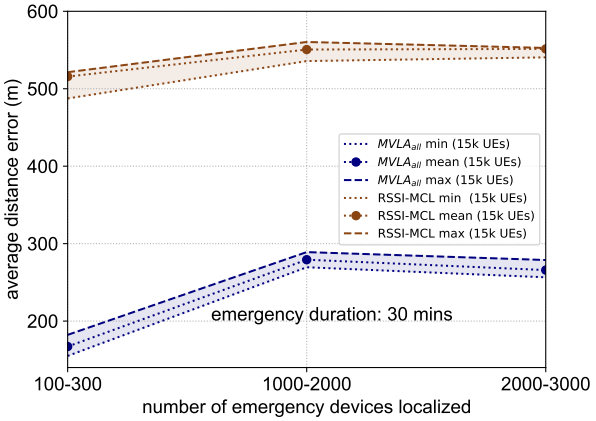

(b) Comparison of ADE achieved under *MVLA*$_{\text{all}}$ and *RSSI-MCL* against the number of victims.

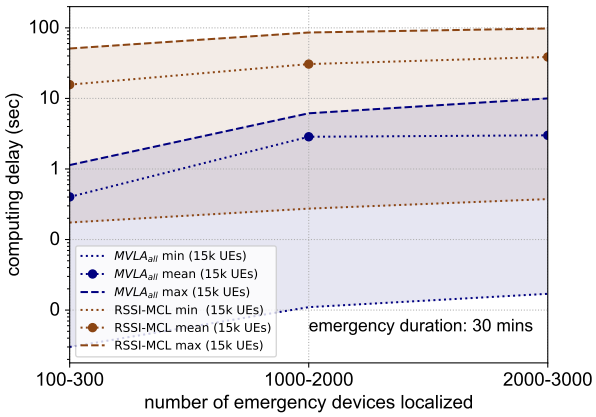

(c) Comparison of computing delay under *MVLA*$_{\text{all}}$ and *RSSI-MCL* against the number of victims.

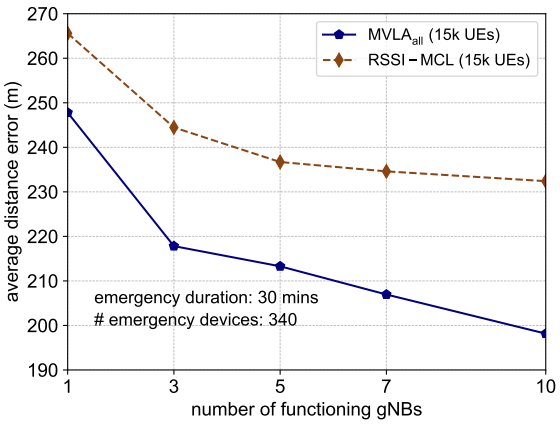

(d) Comparison of ADE under *MVLA*$_{\text{all}}$ and *RSSI-MCL* against the number of functioning gNBs. Total number of gNBs in the area (including broken gNBs) = 39.

Figure 13: Comparison of $MVLA_{all}$ against *RSSI-MCL*. Parameters: R_{min} = 2 m, R_{max} = 1000 m, α_{RSSI} = 0.8, α_{ToA} = 0.2, α_{AoA} = 30^0. Localization approach: GPS+RSSI+AoA+ToA. Emergency calls occurring duration = 30 minutes. The minimum and maximum error limits of each scheme are denoted by the upper and lower bounds of the filled region with its distinct color. gNB distribution is as in Figure 9a.

Tabu Search, etc.) or Decision Tree exploration-based methods [66] such as Branch and Bound or Branch and Cut can be used.

IV. Conclusion and Future Directions

This paper presented the localization mechanism of victims using data received over multi-hop emergency calls from in-coverage and out-of-coverage areas during a disaster. Hence, real-time multi-emergency device localization modes based on dynamic constraints satisfaction method were proposed. The simulations demonstrated that the $MVLA_{all}$ approach allowed to localize up to around 2500 victims in less than 10 seconds and improved localization accuracy by 55.9% compared to *RSSI-MCL*. In a more dense city with a higher number of victims, two alternative modes, called $MVLA_{seq}$ and $MVLA_{recent}$, can be used to reduce response delay with a trade-off of lower localization accuracy than $MVLA_{all}$. One of the major advantages provided by our approach is the management of the trade-off between localization accuracy and system responsiveness. It is then interesting to study how the constraints linearization improvement may impact the localization accuracy without increasing the DCSP complexity. Currently, GPS, RSSI and ToA constraints are approximated using square areas. The study of other polygonal shapes that reduces the feasible area extension is one of the first steps in the improvement of the method. Additionally, the localization of moving devices using the proposed approach can be an interesting area for future research, which requires considering constraints related to the reception time of data, as the victim or relay devices involved are not in the same position. In such scenarios, optimization approaches like Meta-heuristics or Decision Tree exploration-based methods should be used to prioritize constraints based on their freshness. Furthermore,

methods such as particle filtering are suitable for localizing multiple mobile victims due to its ability to track continuous position changes.

REFERENCES

[1] G. Krüger, R. Springer, and W. Lechner, "Global navigation satellite systems (gnss)," *Comput. Electron. Agric.*, vol. 11, no. 1, pp. 3–21, 1994, global Positioning Systems in Agriculture.

[2] J. Paziewski, "Recent advances and perspectives for positioning and applications with smartphone GNSS observations," *Measurement Science and Technology*, vol. 31, no. 9, p. 091001, jun 2020.

[3] S. Verhagen, "Performance analysis of gps, galileo and integrated gps-galileo," 01 2002, pp. 2208–2215.

[4] R. Li, S. Zheng, E. Wang, J. Chen, S. Feng, D. Wang, and L. Dai, "Advances in beidou navigation satellite system (bds) and satellite navigation augmentation technologies," *Satellite Navigation*, vol. 1, p. 12, 03 2020.

[5] L. Dong, H. Ling, and R. Heath, "Multiple-input multiple-output wireless communication systems using antenna pattern diversity," 12 2002, pp. 997 – 1001 vol.1.

[6] R. Hussain, A. Alreshaid, S. Podilchak, and M. Sharawi, "A compact 4g mimo antenna integrated with a 5g array for current and future mobile handsets," *IET Microwaves, Antennas & Propagation*, vol. 11, 02 2017.

[7] H. Du, C. Zhang, Q. Ye, W. Xu, P. Kibenge, and K. Yao, "A hybrid outdoor localization scheme with high-position accuracy and low-power consumption," *EURASIP J Wirel Commun Netw.*, vol. 2018, 01 2018.

[8] A. Hertelendy, K. Goniewicz, and A. Khorram-Manesh, "The applications of geographic information systems in disaster and emergency management in europe," *Disaster and Emergency Medicine Journal*, 10 2020.

[9] E. Cabral, W. Castro, D. Florentino, D. Viana, J. Costa Júnior, R. Souza, A. Rêgo, I. Araújo-Filho, and A. Medeiros, "Response time in the emergency services. systematic review," *Acta Cirurgica Brasileira*, vol. 33, pp. 1110–1121, 12 2018.

[10] D. W. Griffith, F. J. Cintrón, and R. A. Rouil, "Physical sidelink control channel (pscch) in mode 2: Performance analysis," in *2017 IEEE International Conference on Communications (ICC)*, 2017, pp. 1–7.

[11] H. Yoon, R. Shiftehfar, S. Cho, B. Spencer, M. Nelson, and G. Agha, "Victim localization and assessment system for emergency responders," *Journal of Computing in Civil Engineering*, vol. 30, p. 04015011, 03 2016.

[12] J. Han and J. Han, "Building a disaster rescue platform with utilizing device-to-device communication between smart devices," *International Journal of Distributed Sensor Networks*, vol. 14, p. 155014771876428, 03 2018.

[13] C. Pu and X. Zhou, "Rescueme: Smartphone-based self rescue system for disaster rescue," *2019 IEEE 9th Annual Computing and Communication Workshop and Conference (CCWC)*, pp. 0832–0837, 2019.

[14] V. Basnayake, H. Mabed, D. N. K. Jayakody, and P. Canalda, "M-help - multi-hop emergency call protocol in 5g," in *2020 IEEE 19th International Symposium on Network Computing and Applications (NCA)*, 2020, pp. 1–8.

[15] V. Basnayake, H. Mabed, D. N. K. Jayakody, P. Canalda, and M. Beko, "Adaptive emergency call service for disaster management," *Journal of Sensor and Actuator Networks*, vol. 11, no. 4, 2022. [Online]. Available: https://www.mdpi.com/2224-2708/11/4/83

[16] A. Thomas and G. Raja, "Finder: A d2d based critical communications framework for disaster management in 5g," *Peer-to-Peer Networking and Applications*, vol. 12, pp. 912–923, 07 2019.

[17] E. Colle and S. Galerne, "Mobile robot localization by multiangulation using set inversion," *Robotics and Autonomous Systems*, vol. 61, p. 39–48, 01 2013.

[18] K. Merry and P. Bettinger, "Smartphone gps accuracy study in an urban environment," *PLOS ONE*, vol. 14, no. 7, pp. 1–19, 07 2019. [Online]. Available: https://doi.org/10.1371/journal.pone.0219890

[19] M. B. Kjærgaard, H. Blunck, T. Godsk, T. Toftkjær, D. Christensen, and K. Grønbæk, "Indoor positioning using gps revisited," in *Pervasive*, 2010.

[20] J. Arias, A. Zuloaga, J. Lázaro, J. Andreu, and A. Astarloa, "Malguki: An rssi based ad hoc location algorithm," *Microprocessors and Microsystems*, vol. 28, pp. 403–409, 10 2004.

[21] R. Mehra and A. Singh, "Real time rssi error reduction in distance estimation using rls algorithm," in *2013 3rd IEEE International Advance Computing Conference (IACC)*, 2013, pp. 661–665.

[22] M. Dashti, M. Ghoraishi, K. Haneda, and J.-i. Takada, "Sources of toa estimation error in los scenario," in *2010 IEEE International Conference on Ultra-Wideband*, vol. 2. IEEE, 2010, pp. 1–4.

[23] M. Schüssel, "Angle of arrival estimation using wifi and smartphones," 2016.

[24] "Gps.gov: Gps accuracy," (Accessed on 07/28/2021). [Online]. Available: https://www.gps.gov/systems/gps/performance/accuracy/

[25] F. Zahradnik, "Gps smartphone apps vs. dedicated car gps devices," https://www.lifewire.com/smartphone-or-car-gps-1683388, July 2021, (Accessed on 08/15/2021).

[26] T. Geok, K. Aung, M. Aung, M. Soe, A. Abdaziz, C. Liew, F. Hossain, C. Tso, and W. Yong, "Review of indoor positioning: Radio wave technology," *Applied Sciences*, vol. 11, p. 279, 12 2020.

[27] C. Dunphy, "5g goes mainstream: Apple's iphone 12 debuts - mobile internet resource center," https://www.rvmobileinternet.com/5g-goes-mainstream-apples-iphone-12-debuts/, (Accessed on 08/16/2021).

[28] M. Sauter, "From gsm to lte-advanced: An introduction to mobile networks and mobile broadband: Second edition," pp. 1–441, 01 2014.

[29] Z. Xiao and Y. Zeng, "An overview on integrated localization and communication towards 6g," 06 2020.

[30] I. Vin, D. P. Gaillot, P. Laly, M. Liénard, and P. Degauque, "Overview of mobile localization techniques and performances of a novel fingerprinting-based method," *Comptes Rendus Physique*, vol. 16, no. 9, pp. 862–873, 2015, radio science for connecting humans with information systems / L'homme connecté. [Online]. Available: https://www.sciencedirect.com/science/article/pii/S1631070515001929

[31] A. Chatzimichail, A. Tsanousa, G. Meditskos, S. Vrochidis, and I. Kompatsiaris, *RSSI Fingerprinting Techniques for Indoor Localization Datasets*, 09 2020, pp. 468–479.

[32] F. Shang, W. Su, Q. Wang, H. Gao, and Q. Fu, "A location estimation algorithm based on rssi vector similarity degree," *International Journal of Distributed Sensor Networks*, vol. 2014, pp. 1–22, 08 2014.

[33] J. A. del Peral-Rosado, R. Raulefs, J. López-Salcedo, and G. Seco-Granados, "Survey of cellular mobile radio localization methods: From 1g to 5g," *IEEE Communications Surveys & Tutorials*, vol. 20, pp. 1124–1148, 2018.

[34] M. Laaraiedh, "Contributions on hybrid localization techniques for heterogeneous wireless networks," Ph.D. dissertation, 12 2010.

[35] M. W. Khan, N. Salman, A. H. Kemp, and L. Mihaylova, "Localisation of sensor nodes with hybrid measurements in wireless sensor networks," *Sensors*, vol. 16, no. 7, 2016. [Online]. Available: https://www.mdpi.com/1424-8220/16/7/1143

[36] C. Geng, T. Abrudan, V. M. Kolmonen, and H. Huang, "Experimental study on probabilistic toa and aoa joint localization in real indoor environments," 02 2021.

[37] S. Kang, T. Kim, and W. Chung, "Hybrid rss/aoa localization using approximated weighted least square in wireless sensor networks," *Sensors*, vol. 20, no. 4, 2020. [Online]. Available: https://www.mdpi.com/1424-8220/20/4/1159

[38] M. Bertoni, S. Michieletto, R. Oboe, and G. Michieletto, "Indoor visual-based localization system for multi-rotor uavs," *Sensors*, vol. 22, no. 15, 2022. [Online]. Available: https://www.mdpi.com/1424-8220/22/15/5798

[39] W. Wang and Q. Zhu, "Rss-based monte carlo localisation for mobile sensor networks," *Communications, IET*, vol. 2, pp. 673 – 681, 06 2008.

[40] A. Krishna, A. van Schaik, and C. S. Thakur, "Source localization using particle filtering on fpga for robotic navigation with imprecise binary measurement," *arXiv preprint arXiv:2010.11911*, 2020.

[41] J. Lu and C. C. Wang, "A new monte carlo mobile node localization algorithm based on newton interpolation," *EURASIP Journal on Wireless Communications and Networking*, vol. 2018, pp. 1–8, 2018.

[42] C. Zhou, H. Tian, and B. Zhong, "An improved mcb localization algorithm based on weighted rssi and motion prediction," *Computer Science and Information Systems*, vol. 17, pp. 779–794, 01 2020.

[43] G. Li, J. Zhang, J. Chen, and Z. Xu, "A monte carlo box localization algorithm based on rssi," in *Proceedings of the 33rd Chinese Control Conference*, 2014, pp. 395–400.

[44] K. Kueviakoe, Z. Wang, A. Lambert, E. Frenoux, and P. Tarroux, "Localization of a vehicle: A dynamic interval constraint satisfaction problem-based approach," *Journal of Sensors*, vol. 2018, pp. 1–12, 04 2018.

[45] B. Abbache, N. Roumila, S. Rezzoug, M. Omar, and A. Tari, "Collaborative localization algorithm based on constraint programming," in *Proceedings of the International Conference on Big Data and Advanced Wireless Technologies*, ser. BDAW '16. New York, NY, USA: Association for Computing Machinery, 2016. [Online]. Available: https://doi.org/10.1145/3010089.3010104
[46] F. Mourad, H. Snoussi, F. Abdallah, and C. Richard, "Anchor-based localization via interval analysis for mobile ad-hoc sensor networks," *IEEE Transactions on Signal Processing*, vol. 57, no. 8, pp. 3226–3239, 2009.
[47] E. Colle and S. Galerne, "Mobile robot localization by multiangulation using set inversion," *Robotics and Autonomous Systems*, vol. 61, no. 1, pp. 39–48, 2013.
[48] M. Qin and R. Zhu, "A monte carlo localization method based on differential evolution optimization applied into economic forecasting in mobile wireless sensor networks," *EURASIP Journal on Wireless Communications and Networking*, vol. 2018, 02 2018.
[49] A. abu znaid, M. Yamani, M. Idris, A. Wahid, A. Wahab, L. Qabajeh, and O. MAHDI, "Sequential monte carlo localization methods in mobile wireless sensor networks: A review," *Journal of Sensors*, vol. 2017, 04 2017.
[50] D. C. Yuen and B. A. MacDonald, "A comparison between extended kalman filtering and sequential monte carlo techniques for simultaneous localisation and map-building," in *Proceedings of the 2002 Australasian Conference on Robotics and Automation*. Citeseer, 2002, pp. 111–116.
[51] A. Singh, "Extended kalman filter. in my previous blog i have covered… — by atul singh — towards data science," https://towardsdatascience.com/extended-kalman-filter-ee9bd04ac5dc, May 2018, (Accessed on 08/31/2021).
[52] F. Mourad, H. Snoussi, F. Abdallah, and C. Richard, "Anchor-based localization via interval analysis for mobile sensor networks," *IEEE Transactions on Signal Processing*, vol. 57, no. 8, pp. 3226–3239, 2009.
[53] M. Kieffer, L. Jaulin, E. Walter, and D. Meizel, "Robust autonomous robot localization using interval analysis," *Reliable Computing*, vol. 6, pp. 337–362, 08 2000.
[54] Z. Wang and A. Lambert, "A low-cost consistent vehicle localization based on interval constraint propagation," *Journal of Advanced Transportation*, vol. 2018, 06 2018.
[55] F. Mourad, H. Snoussi, F. Abdallah, and C. Richard, "Guaranteed boxed localization in manets by interval analysis and constraints propagation techniques," in *IEEE GLOBECOM 2008 - 2008 IEEE Global Telecommunications Conference*, 2008, pp. 1–5.
[56] V. Drevelle and P. Bonnifait, "Robust positioning using relaxed constraint-propagation," in *2010 IEEE/RSJ International Conference on Intelligent Robots and Systems*, 2010, pp. 4843–4848.
[57] M. Mouhoub and B. Jashmi, "Heuristic techniques for variable and value ordering in csps," 01 2011, pp. 457–464.
[58] S. Mintonl, M. Johnston, A. B. Philips, and P. Laird, "Stolving large-scale constraint satisfaction an scheduling problems using a epair metho," 1990.
[59] M. Wahbi, *Algorithms and Ordering Heuristics for Distributed Constraint Satisfaction Problems*, 06 2013.
[60] F. Mourad, H. Snoussi, and C. Richard, "Interval-based localization using rssi comparison in manets," *IEEE Transactions on Aerospace and Electronic Systems*, vol. 47, no. 4, pp. 2897–2910, 2011.
[61] J. Fernández, M. Quispe, G. Kemper, J. Samaniego, and D. Diaz, "An improvement of the log-distance path loss model for digital television in lima," *XXX Simposio Brasilero de Telecomunications*, 09 2012.
[62] F. Palacios-Gomez, L. Lasdon, and M. Engquist, "Nonlinear Optimization by Successive Linear Programming," *Management Science*, vol. 28, no. 10, pp. 1106–1120, Oct. 1982, publisher: INFORMS.
[63] S. Rohou *et al.*, "The Tubex library – Constraint-programming for robotics," 2017, http://simon-rohou.fr/research/tubex-lib/.
[64] E. Bisong, *Google Colaboratory*. Berkeley, CA: Apress, 2019, pp. 59–64.
[65] E.-G. Talbi, *Metaheuristics: from design to implementation*. John Wiley & Sons, 2009.
[66] R. Kabra and R. Bichkar, "Performance prediction of engineering students using decision trees," *International Journal of computer applications*, vol. 36, no. 11, pp. 8–12, 2011.

Vishaka Basnayake received her B.Sc. degree in Electrical and Electronic Engineering from University of Peradeniya, Sri Lanka in 2017 and M.Sc. degree in Wireless Communication Engineering from University of Oulu, Finland, in 2019. She is currently pursuing a Ph.D. degree at Universite Bourgogne Franche Comte (UBFC), France in collaboration with Sri Lanka Technological Campus (SLTC), Sri Lanka. Her research interests include D2D communication in cellular wireless networks, Asynchronous NOMA, Optimization, Localization, Network protocol design and Distributed learning.

Hakim Mabed is an associate professor at the University of Bourgogne Franche-Comté (UBFC), France. He is part of the FEMTO-ST institute (UMR CNRS 6174) and the complex networks team where he does his research. He obtained the Ph.D. degree from the University of Angers, France in 2003; he received the M.S. degree from the University of Algiers, Algeria in 2000. His research interests cover many fields such as distributed intelligent MEMS, wireless communications, combinatorial optimization, and programmable matter. He led and participate to different funded research projects (SOES, ALGOPDF, WIFIOPT) in collaboration with THALES, Orange Lab. and DGA. He has authored and co-authored more than 60 international publications.

Philippe Canalda received his Ph.D (1997) from the INRIA Research Centre and the University of Orléans. He worked 2 years in the Associated Compiler Expert start-up on optimization engines, then 2 years at LORIA research institute on synchronized and complex processes. Since 2001, as assistant professor at UFC he is focusing on continuity of positioning in indoor and outdoor environments on the one part, and on the other part on dynamic itinerary generation and the integration of on-demand transportation service (carpooling, car-sharing) in a global public and multi-modal transportation offer. He's teaching in and co-managing an international master Internet of Things in Advanced Networks and Computer Science.

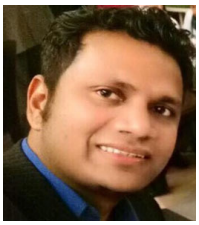

Dushantha Nalin K. Jayakody (S'09, M'14, SM' 18) is a Senior Member IEEE, Fellow, IET, and received his Ph.D. in Electronics and Communications Engineering, from the University College Dublin, Ireland in 2013. Since 2021, he is with the Autónoma TechLab, Portugal and Department of Engineering and Computer Science, Universidade Autónoma de Lisboa, Portugal. Prof. Jayakody has published nearly 200 international peer reviewed journal and conference papers and books. His research interests include PHY and NET layer prospective of 5G communications technologies such as NOMA for 5G etc, Cooperative wireless communications, device to device communications, LDPC codes, Unmanned Aerial Vehicle etc. He currently serves as an Area Editor of the Elsevier Physical Communications Journal, MDPI Information journal, MDPI Sensors and Wiley Internet of Technology Letters. Also, he serves on the Advisory Board of MDPI Multidisciplinary Journal Sci. In addition, he serves as a reviewer for various IEEE Transactions and other journals.